# Phase diagram and thermodynamics of the three-dimensional Bose-Hubbard model

B. Capogrosso-Sansone,[1] N. V. Prokof'ev,[1,2,3] and B. V. Svistunov[1,3]
[1]*Department of Physics, University of Massachusetts, Amherst, Massachusetts 01003, USA*
[2]*BEC-INFM, Dipartimento di Fisica, Universitá di Trento, Via Sommarive 14, I-38050 Povo, Italy*
[3]*Russian Research Center "Kurchatov Institute," 123182 Moscow, Russia*
(Received 9 January 2007; published 16 April 2007)

We report results of quantum Monte Carlo simulations of the Bose-Hubbard model in three dimensions. Critical parameters for the superfluid-to-Mott-insulator transition are determined with significantly higher accuracy than has been done in the past. In particular, the position of the critical point at filling factor $n=1$ is found to be at $(U/t)_c=29.34(2)$, and the insulating gap $\Delta$ is measured with accuracy of a few percent of the hopping amplitude $t$. We obtain the effective mass of particle and hole excitations in the insulating state—with explicit demonstration of the emerging particle-hole symmetry and relativistic dispersion law at the transition tip—along with the sound velocity in the strongly correlated superfluid phase. These parameters are the necessary ingredients to perform analytic estimates of the low temperature ($T \ll \Delta$) thermodynamics in macroscopic samples. We present accurate thermodynamic curves, including these for specific heat and entropy, for typical insulating ($U/t=40$) and superfluid ($t/U=0.0385$) phases. Our data can serve as a basis for accurate experimental thermometry, and a guide for appropriate initial conditions if one attempts to use interacting bosons in quantum information processing.

DOI: 10.1103/PhysRevB.75.134302 PACS number(s): 03.75.Hh, 03.75.Lm, 75.40.Mg

## I. INTRODUCTION

In the past decade, strongly correlated lattice quantum systems have been attracting a lot of interest and effort. Remarkably, simple yet nontrivial models which contain most of the important many-body physics and known in the theory community for many years can be now realized and studied experimentally. Theoretical predictions and experimental data for strongly correlated states can be directly tested against each other in the ideal setup when all model ingredients are known and controlled.

Experimentally, lattice systems are realized by trapping atoms in an optical lattice, a periodic array of potential wells resulting from the dipole coupling of the atoms to the electric field of the standing electromagnetic wave produced by a laser. Optical lattices are a very powerful and versatile tool. By changing the laser parameters and configuration, the properties and geometry of the optical lattice can be finely tuned.[1] Ultimately, this results in the possibility of controlling the Hamiltonian parameters and exploring various regimes of interest. In particular, ultracold Bose atoms trapped in an optical lattice are an experimental realization of the Bose-Hubbard model. The model has been studied in the seminal paper by Fisher, Weichman, Grinstein, and Fisher[2] and its physical realization with ultracold atoms trapped in an optical lattice has been envisioned in Ref. 3. A few years later, the Bose-Hubbard system was produced in the laboratory.[4] Since then, the field remains very active,[5–10] not only because theoretical predictions and experimental techniques still have to be substantially improved to claim the quantitative agreement, but also because of the new physical applications.

At zero temperature, a system of bosons with commensurate filling factor undergoes a superfluid-to-Mott-insulator (SF-MI) quantum phase transition. The ground state of MI can be used in quantum information processing to initialize a large set of qubits (the main remaining challenge is in addressing single atoms to build quantum gates, see Ref. 1, and references therein). Atomic systems in optical lattices have the advantage of being well isolated from the environment. This results in a relatively long decoherence time of the order of seconds[1] and therefore the possibility of building long-lived entangled many body states. These properties make MI ground states good candidates for building blocks of a quantum computer. Another possible application is in interferometric measurements.[11] It has been argued[12–14] that using the superfluid-to-Mott-insulator phase transition to entangle and disentangle atomic Bose-Einstein condensate one can go beyond the Heisenberg-limited interferometry.

A system of bosons with short-range repulsive pair interaction trapped in an optical lattice is described by the Bose-Hubbard Hamiltonian

$$H = -t\sum_{\langle ij\rangle} b_i^\dagger b_j + \frac{U}{2}\sum_i n_i(n_i-1) - \sum_i \mu_i n_i, \qquad (1)$$

where $b_i^\dagger$ and $b_i$ are the bosonic creation and annihilation operators on the site $i$, $t$ is the hopping matrix element, $U$ is the on-site repulsion, and $\mu_i=\mu-V(i)$ is the sum of the chemical potential $\mu$ and the confining potential $V(i)$. In what follows, we consider bosons in the simple cubic lattice. At zero temperature and integer filling factor, the competition between kinetic energy and on-site repulsion induces the MI-SF transition. When the on-site repulsion is dominating, $t/U \ll 1$ the atoms are tightly localized in the MI ground state which is well approximated by the product of local (on-site) Fock states. The Mott state is characterized by zero compressibility originating from an energy gap for particle and hole excitations. When the hopping amplitude is increased up to a certain critical value $(t/U)_c$, particle delocalization becomes energetically more favorable and the system Bose condenses. In the chemical potential vs hopping matrix element plane (energies are scaled by $U$), the $T=0$ phase diagram has a characteristic lobe shape,[2] see also Fig. 3 below, with the MI phase being inside the lobe (there is one lobe for

 

each integer filling factor). The most interesting region in the phase diagram is the vicinity of the lobe tip ($\mu=\mu_c$, $t=t_c$) corresponding to the MI-SF transition in the commensurate system. For other values of $\mu$ or $t$, the SF-MI criticality is trivial and corresponds to the weakly interacting Bose gas at vanishing particle density.[2] It is straightforward to describe provided the particle (hole) effective mass is known. If, however, one crosses the MI-SF boundary at constant commensurate density (this is equivalent to going through the tip of the lobe at a fixed chemical potential) the long-wave action of the system becomes relativistic and particle-hole symmetric. Now the phase transition is in the four-dimensional U(1) universality class.[2] It is worth emphasizing that here we have a unique opportunity of a laboratory realization of the nontrivial relativistic vacuum, a sort of a "hydrogen atom" of strongly interacting relativistic quantum fields. Approaching the critical point from the MI side, one deals with the vacuum that supports massive bosonic particles and antiparticles (particles and holes). On the other side of the transition, the SF vacuum supports massless bosons (phonons) that do not have an antiparticle analog. In principle, one can systematically study universal multiparticle scattering amplitudes of the relativistic quantum field theory in the ultracold "supercollider."

The present study is focused on the three-dimensional (3D) system. To the best of our knowledge, previous systematic studies of the 3D case were limited to the mean-field[2] (MF) and perturbative methods.[15] In Ref. 15, the authors utilized the strong-coupling expansion to establish boundaries of the phase diagram in the $(\mu/U, t/U)$ plane. This approach, based on the small ratio $zt/U \ll 1$, where $z=6$ is the coordination number for the simple cubic lattice, works well only in the MI phase in the region far from the tip of the lobe, where the insulating gap is larger then hopping $\Delta/zt > 1$. Close to the critical region, where $\Delta/zt \sim 1$, the strong-coupling expansion is no longer valid. We present the results of large-scale Monte Carlo (MC) simulations of the model (1) by the worm algorithm.[16] With precise data for the single-particle Green function, we are able to carefully trace the critical and close-to-critical behavior of the system, and, in particular, produce an accurate phase diagram in the region of small insulating gaps $\Delta \ll t$. Though the corresponding parameter range is quite narrow, it is crucial to clearly resolve it to reveal the emerging particle-hole symmetry and relativistic long-wave physics at the tip of the MI-SF transition. We also present data for the effective masses of particle and hole excitations inside the insulating phase. Close to the MI lobe tip, the data for the dispersion of the elementary excitations are fitted by the relativistic law, in agreement with the theory (this also allows us to extract the value of the sound velocity in the critical region). In the Mott state, the knowledge of gaps and effective masses is sufficient to calculate the partition function in the low temperature limit analytically and to make reliable predictions for the system entropy.

For such applications of the system as quantum information processing and interferometry, controlling the temperature is of crucial importance. Most applications are based on the key property of the good insulating state, which is small density fluctuations in the ground state. At zero temperature fluctuations are of quantum nature and can be efficiently controlled externally through the $t/U$ ratio. At finite temperature, fluctuations are enhanced by thermally activated particle-hole excitations. Only when the temperature is much smaller than the energy gap, the number of excitations is exponentially small. Up to date, there are no available experimental techniques to measure the temperature of a strongly interacting system. For weakly interacting systems, the temperature can be extracted in a number of ways, e.g., from the interference pattern of matter waves[17] or the condensate fraction observed after the trap is released and the gas expands freely[18]—these properties are directly related to the momentum distribution function $n(\mathbf{k})$. For strongly interacting systems, both temperature and interaction are responsible for filling the higher momentum states, which makes it hard to extract temperature using absorption imaging techniques.

The results presented in this paper can be used to perform accurate thermometry. Typically, the initial temperature $T^{(\mathrm{in})}$ (before the optical lattice is adiabatically loaded) is known. By entropy matching one can easily deduce the final temperature of the MI state $T=T^{(\mathrm{fin})}$, provided the entropy of the MI phase is known. To this end we have calculated the energy, specific heat, and entropy of the system in several important regimes which include MI and strongly correlated SF phases. These data can be used to suggest appropriate initial conditions which make the Bose-Hubbard system suitable for physical applications, such as the ones described above.

Another interesting question concerns the nature of inhomogeneous states in confined systems when the MI phase is formed in the trap center. The confining potential provides a scan in the chemical potential of the phase diagram at fixed $t/U$ (see Ref. 3). As one moves away from the trap center the system changes its local state. At zero temperature, the density profile of the system can be read (up to finite-size effects) from the ground state phase diagram. At finite temperature, this is no longer possible. In particular, the liquid regions outside of the MI lobes could be normal or superfluid, depending on temperature.

So far experimental results have been interpreted by assuming that liquid regions are superfluid, but there were no direct measurements or calculations to prove that this was the case. [Part of the problem is that absorption imaging is sensitive only to $n(\mathbf{k})$, which is the Fourier transform of the single-particle density matrix in the relative coordinate. All parts of the system contribute to $n(\mathbf{k})$ and it is hard to discriminate where the dominant contribution comes from.] It is almost certain that $T^{(\mathrm{fin})}/T_c^{(\mathrm{fin})}$ of the strongly correlated system is higher then $T^{(\mathrm{in})}/T_c^{(\mathrm{in})}$. Indeed, since the entropy of MI at $\Delta \gg T$ is exponentially small, most entropy will be concentrated in the liquid regions. At this point we notice that the transition temperature in the liquid is suppressed relative to the noninteracting Bose gas value $T_c^{(0)} \approx 3.313 n^{2/3}/m$ by both (i) effective mass enhancement in the optical lattice, $m \to 1/2ta^2$ (here $a$ is the lattice constant) and (ii) strong repulsive interactions in the vicinity of the Mott phase, in fact, $T_c \to 0$ at the SF-MI boundary. It seems plausible that the MI phase is always surrounded by a broad normal liquid (NL) region. It may also happen that superfluidity is completely eliminated in the entire sample in the final state. [Strictly

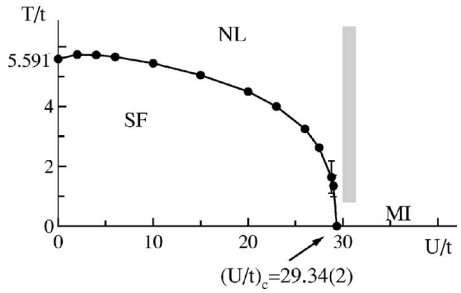


FIG. 1. Finite-temperature phase diagram at filling factor $n=1$. Solid circles are simulation results (the line is a guidance for the eye), error bars are plotted. $T=5.591t$ is the critical temperature of the ideal Bose gas with the tight binding dispersion relation. At finite, but low enough temperature, the MI domain is loosely defined as the part of the phase diagram to the right of the gray line. The rest of the nonsuperfluid domain is referred to as normal liquid (NL).

speaking, at $T\neq 0$ the MI and NL phases are identical in terms of their symmetries and are distinguished only *quantitatively* in the density of particle-hole excitations, i.e., in the Hamiltonian (1) the finite-temperature MI is continuously connected without phase transition to NL, see Fig. 1. For definiteness, we will call NL a normal finite-$T$ state which is superfluid at $T=0$ for the same set of the Hamiltonian parameters.] Figure 1 shows the finite-temperature phase diagram (see also Ref. 19) for filling factor $n=1$ (we will discuss how we determine the critical temperature in Sec. III). The critical temperature goes to zero sharply, while approaching the critical point. In the limit of $U\rightarrow 0$ the critical temperature is slightly above the ideal-gas prediction ($T=5.591t$ was calculated using the tight binding dispersion relation), as expected (see, e.g., Ref. 20).

The paper is organized as follows. In Sec. II we present results for the ground-state phase diagram and effective mass of particle (hole) excitations, at integer filling factor $n=1$. In Sec. III we investigate the thermodynamic properties of the system. We present data for energy, specific heat, and entropy and calculate the final temperature of the uniform and harmonically confined system in the limit of large gaps. For the case of trapped system, we also determine the state of the liquid at the perimeter of the trap. Brief conclusions are presented in Sec. IV.

## II. GROUND-STATE PROPERTIES

This section deals with the results of large-scale Monte Carlo simulations for the ground state phase diagram of the Bose-Hubbard system in three dimensions. Analytical approaches, e.g., the strong coupling expansion, work well in the region where $zt/U\ll 1$ and the system is deep in the MI phase. Under these conditions the kinetic energy term in the Hamiltonian can be treated perturbatively and the unperturbed ground state is a product of local Fock states. In Ref. 15 the authors carried out an expansion, up to the third order in $zt/U$, for the SF-MI boundaries and estimated positions of critical points at the tips of the MI lobes (by extrapolating results to the infinite expansion order). Their results agree with the mean field solution calculated in Ref. 2, when the latter is expanded up to the third order in $zt/U$ and the dimension of space goes to infinity. As already mentioned, this approach starts failing when $\Delta\sim zt$. Using MC techniques we were able to calculate critical parameters and predict the position of the diagram tip with much higher accuracy: with the worm algorithm (WA) approach the energy gaps can be measured with precision of the order of $10^{-2}t$ (see Ref. 21). The simulation itself is based on the configuration space of the Matsubara Green function

$$G(i,\tau)=\langle \mathcal{T}_\tau b_i^\dagger(\tau)b_0(0)\rangle, \tag{2}$$

which is thus directly available. We utilize the Green function to determine dispersion relations for particle and hole excitations at small momenta [from the exponential decay of $G(\mathbf{p},\tau)$ with the imaginary time] which directly give us the energy gap and effective masses.

Recall that in the momentum space the Green function of a finite size system $G(\mathbf{p},\tau)$ is different from zero only for $\mathbf{p}=\mathbf{p_m}=2\pi(m_x/L_x,m_y/L_y,m_z/L_z)$, where $L_{\alpha=x,y,z}$ is the linear system size in direction $\alpha$ (we performed all simulations in the cubic system with $L_\alpha=L$), and $\mathbf{m}=(m_x,m_y,m_z)$ is an integer vector. Using Lehman expansion and extrapolation to the $\tau\rightarrow\pm\infty$ limit one readily finds that

$$G(\mathbf{p},\tau)\rightarrow\begin{cases} Z_+e^{-\epsilon_+(\mathbf{p})\tau}, & \tau\rightarrow+\infty, \\ Z_-e^{\epsilon_-(\mathbf{p})\tau}, & \tau\rightarrow-\infty. \end{cases} \tag{3}$$

The two limits describe single-particle/hole excitations in the MI phase. Here $Z_\pm$ and $\epsilon_\pm$ are the particle/hole spectral weight (or $Z$ factors) and energy, respectively. In the grand canonical ensemble, excitation energies are measured relative to the chemical potential. With this in mind, calculating the phase diagram of the system is rather straightforward. At a fixed number of particles $N=L^3$ and $t/U$ ratio one determines chemical potentials $\mu_\pm$ for which the energy gap for creating the particle/hole excitation with $\mathbf{p}=0$ vanishes. The insulating gap is given then by $\Delta=\mu_+-\mu_-$. For high precision simulations of the gap one has to choose the value of $\mu$ very close to $\mu_\pm$ and consider finite, but zero for all practical purposes, value of temperature so that the following two conditions are satisfied:

$$|\mu-\mu_\pm|\ll t, \quad |\mu-\mu_\pm|\gg T. \tag{4}$$

This is exactly how we proceed. By plotting $\ln[G(\mathbf{p},\tau)]$ vs $\tau$ we deduce $\epsilon_\pm(\mathbf{p})$ from the exponential decay of the Green function. A typical example is shown in Fig. 2. We use the values of the hopping amplitude $t$ and the lattice constant $a$ as units of energy and distance, respectively.

In Fig. 3 we present accurate results for the boundaries of the first Mott insulator lobe. We have done calculations for systems with linear sizes $L=5$, 10, 15, 20. Up to values of $t/U\sim 0.031$ no size effects were detected within the error bars. (Here and throughout the paper error bars are of two standard deviations.) In the critical region the finite-size effects were eliminated using standard scaling techniques (see below). The dashed lines are the prediction of Ref. 15 based on the third-order expansion in $t/U$. It becomes inaccurate quite far from the tip when the insulating gap is about $\sim 6t$.

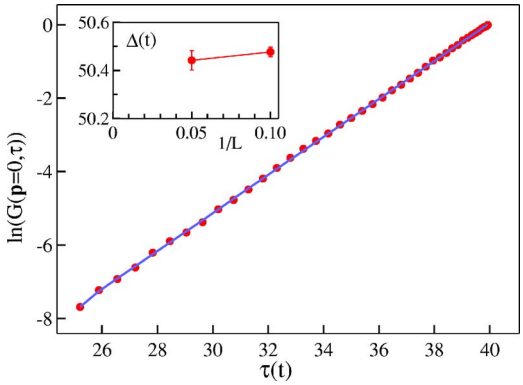


FIG. 2. (Color online) Zero-momentum Green function in the Mott phase with the chemical potential $\mu/U=0.809$, slightly below the upper phase boundary. Here we show data for the system with $N=10^3$ bosons at $U/t=70$ and $T/t=0.025$. In the inset we plot the energy gap $\triangle$ for linear system sizes $L=10$ and 20. Finite-size errors are within the statistical error bars.

On the other hand, the value of the tip position extrapolated to the infinite order is right on target, within the error bar of order $3t$ for the chemical potential and on-site repulsion. In all simulations (performed at $t/T=40$) the finite-temperature effects are negligible—the system is essentially in its ground state.

To eliminate finite-size effects in the critical region and pinpoint the position of the lobe tip, we employed standard scaling techniques based on the universality considerations. First, let us briefly review the universal properties of the insulator-to-superfluid transition (see Ref. 2 for more details). There exist two types of transitions: the "generic" transition, when the phase boundary is crossed at fixed $t/U$, and a special transition at fixed integer density, when the SF-MI boundary is crossed at fixed $\mu/U$. The generic transition is driven by the addition/subtraction of a small number of particles, and is fully characterized by the physics of the weakly interacting Bose gas formed by the small incommensurate density component $n-n_0$, where $n_0$ is the nearest integer to $n$. In particular, if $\delta$ is the deviation from the generic critical

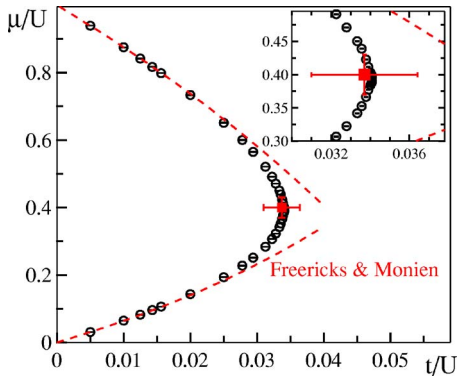


FIG. 3. (Color online) Phase diagram of the first MI-SF lobe. Numerical data are shown by open circles. The error bars are shown but are barely visible even in the inset. The dashed lines and the square represent results of Ref. 15 for the strong coupling expansion and the extrapolated position of the diagram tip, respectively.

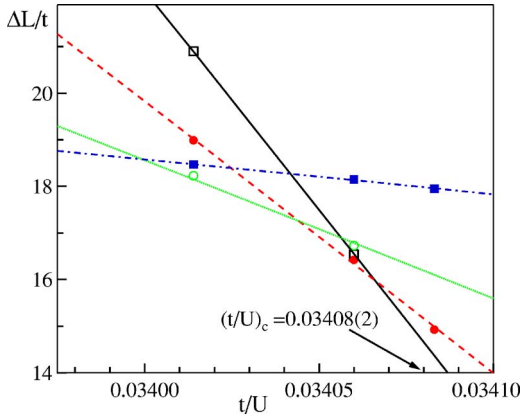


FIG. 4. (Color online) Finite size scaling of the energy gap at the tip of the lobe. $\Delta L/t$ vs $t/U$ for system size $L=5$ (solid squares), $L=10$ (open circles), $L=15$ (solid circles), $L=20$ (open squares). Lines represent linear fits used to extract the critical point.

point in the chemical potential or $t/U$ ratio then $|n-n_0|\sim\delta$ and $T_c(\delta)\sim\delta^{2/3}$ in the SF phase.

The special transition at the tip of the lobe happens at fixed integer density. It is driven by delocalizing quantum fluctuations which for large values of $t/U$ enable bosons to overcome the on-site repulsion and hop within the lattice. As explained in Ref. 2, the effective action for the special transition belongs to the $(d+1)$-dimensional $XY$ universality class which implies emergent relativistic invariance (rotational invariance in the imaginary-time space, which is equivalent to the Lorentz invariance in real-time space) and, in particular, an emergent particle-hole symmetry. The upper critical dimension for this transition is $(d+1)=4$, so that for $d>3$ the critical exponents for the order parameter, $\beta$, and the correlation length, $\nu$, are of mean-field character: $\beta=\nu=1/2$ (with logarithmic corrections for $d=3$). In this study, we were not able to resolve logarithmic renormalizations for realistic 3D systems and proceed below with the analysis which assumes mean-field scaling laws.

Denoting the distance from the critical point as $\gamma=[(t/U)_c-t/U]$, for a system of linear size $L$ one can write

$$\Delta(\gamma,L)=\xi^{-1}f(\xi/L)=L^{-1}g(\gamma L^2), \tag{5}$$

where $\Delta$ is the particle-hole excitation gap, $\xi$ is the correlation length, and $f(x)$ and $g(x)$ are the universal scaling functions. In the last expression we have used the relation $\xi\propto\gamma^{-1/2}$. At the critical point, the product $L\Delta$ does not depend on the system size. Therefore, by plotting $L\Delta$ as a function of $t/U$ one determines the critical point from the intersection of curves referring to different values of $L$, as shown in Fig. 4. This analysis yields (Fig. 5 explains how finite-size effect in the position of the crossing point originating from corrections to scaling was eliminated)

$$(t/U)_c=0.03408(2)\quad(n=1). \tag{6}$$

Our final results are summarized in Fig. 3. We find that the size of the critical region where 4D $XY$ scaling laws apply is narrow and restricted to small gaps of the order of

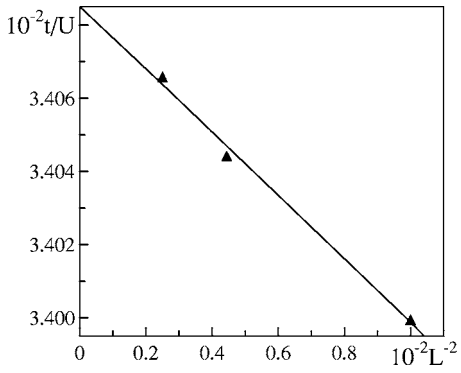


FIG. 5. Extrapolation to the thermodynamic limit. We show the intersections (triangles) of the curves ($L=5$, $L=10$), ($L=10$, $L=15$), ($L=15$, $L=20$), vs $L_{\max}^{-2}$. The fit (solid line) yields $(t/U)_c = 0.03408(2)$.

$\Delta \leqslant t$ (inside the vertical error bar on the strong-coupling expansion result in Fig. 3). It appears that resolving this limit experimentally would be very demanding.

To perform analytic estimates of the MI state energy (and entropy) at low temperature $T \ll \Delta$ one has to know effective masses of particle and hole excitations $m_{\pm}$. For example, the particle/hole contributions to energy in the grand canonical ensemble are given by the sums

$$E_{\pm} = \sum_{\mathbf{k}} \epsilon_{\pm}(\mathbf{k}) n_{\epsilon} \approx \left(\frac{L}{2\pi}\right)^3 \int d\mathbf{k} \epsilon_{\pm}(\mathbf{k}) e^{-\epsilon_{\pm}(\mathbf{k})/T}, \qquad (7)$$

where $n_{\epsilon}$ is the Bose function and

$$\epsilon_{\pm}(\mathbf{k}) \approx \pm(\mu_{\pm} - \mu) + k^2/2m_{\pm}. \qquad (8)$$

For large gaps the tight binding approximation

$$\epsilon_{\pm}(\mathbf{k}) \approx \pm(\mu_{\pm} - \mu) + \sum_{\alpha=x,y,z} \frac{1 - \cos k_{\alpha}}{m_{\pm}} \qquad (9)$$

is a reasonable approximation for all values of $\mathbf{k}$ in the Brillouin zone. Note that, if one is to use the local density approximation (LDA) for the energy/entropy estimates of trapped systems, then calculations have to be performed in the grand canonical ensemble.

To determine effective masses we computed $G(\mathbf{p}, \tau)$ in the insulating state and deduced $\epsilon_{\pm}(\mathbf{p})$ for several lowest momenta from the exponential decay of the Green function on large time scales. Dispersion laws were then fitted by a parabola, with the exception for the diagram tip, where the dispersion relation is relativistic. The result for $m_{\pm}$ is shown in Fig. 6. When $t/U \to 0$ one can calculate effective masses perturbatively in $t/U$ to get

$$tm_{+} = 0.25 - 3t/U, \quad tm_{-} = 0.5 - 12t/U. \qquad (10)$$

Clearly, our data are converging to the analytical result as $t/U \to 0$. On approach to the critical point the effective mass curves become identical for particles and holes indicating that there is an emergent particle-hole symmetry at the diagram tip. In agreement with the theoretical prediction, the data taken at $t/U=0.034$ are fitted best with the relativistic dispersion relation $\varepsilon(p) = c\sqrt{m_*^2 c^2 + p^2}$, where $c$ is the sound velocity and the effective mass is defined as $m_* = \Delta/2c^2$. At this value of $t/U$ we have found that $c/t = 6.3 \pm 0.4$ and $tm_* = 0.010 \pm 0.004$.

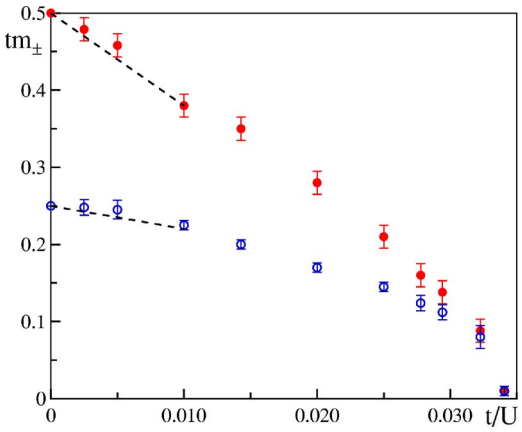


FIG. 6. (Color online) Effective mass for hole (solid circles) and particle (open circles) excitations as a function of $t/U$. The exact results at $t/U=0$ are $m_+ = 0.25/t$ and $m_- = 0.5/t$. By dashed lines we show the lowest order in $t/U$ correction to the effective masses. Close to the critical point the two curves overlap, directly demonstrating the emergence of the particle-hole symmetry. At $t/U = 0.034$, the sound velocity is $c/t = 6.3 \pm 0.4$.

## III. FINITE-TEMPERATURE ANALYSIS

Controlling the temperature is an important experimental issue, crucial for many applications of cold atomic systems and studies of quantum phase transitions. In this section, we discuss thermodynamic properties of the Bose-Hubbard model. We present data for energy, specific heat and entropy, for some specific cases. In particular, we focus on the most important $\langle n \rangle \approx 1$ situation. Our data can be used in two ways: (i) to understand limits of applicability of the semianalytic approach (with calculated effective parameters) discussed above and (ii) to have reference first-principle curves for more refined numerical analysis. Unfortunately, a direct simulation of a realistic case in the trap, i.e., with similar number of particles as in experiments, is still a challenging problem though simulations of about $10^5$ particles or more at low temperature seem feasible in near future.

The results are organized as follows. In Sec. III A we probe the limits of applicability of semianalytic predictions in the Mott state. In Sec. III B we calculate the entropy of the Bose-Hubbard model, compare it to the initial entropy (i.e., before the optical lattice is turned on) and estimate the final temperature. We consider both a homogeneous system in the MI and SF states and a system of $N \sim 3 \times 10^4$ particles in a trap.

### A. Comparison with low-$T$ semianalytic predictions

Away from the tip of the lobe, in the MI state, semianalytic predictions are reliable provided the temperature is low enough, i.e., $T \ll \Delta$. In other words, there exist a range of temperatures, defined as $T \lesssim \text{const}\Delta$, where the quasiparticle excitations can be successfully described as a noninteracting

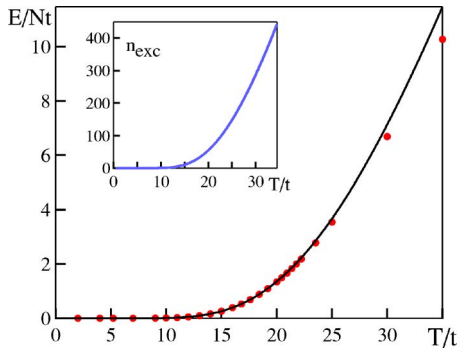


FIG. 7. (Color online). Energy per particle at $t/U=0.005$, unity filling factor and linear system size $L=20$. Solid circles are prime data (error bars within symbol size), the solid line is the analytical prediction from Eq. (7), where, at each temperature, the chemical potential has been fixed by imposing equal number of particle and hole excitations. The inset shows the total number of excitations present in the system.

classical gas [see Eq. (7)]. The value of the constant depends on $\Delta$, as the two following examples demonstrate.

Let us first consider larger gaps, e.g., $\Delta \sim 200t$, for which we have found that the low-temperature analytic predictions reproduce numerical data very well. In Fig. 7 we plot the energy per particle in the low-temperature regime for $\Delta = 181.6t$. The analytic prediction from Eq. (7), where, at any given temperature, the chemical potential has been chosen by setting equal the total number of particle and hole excitations (as it is done for intrinsic semiconductors), is reliable up to temperatures $T \lesssim 35t$, i.e., $T \lesssim 0.15\Delta$. In the inset we plot the average number of particle-hole excitations. This number increases rapidly with temperature justifying the grand-canonical calculation for the quasiparticle gas (at fixed total number of particles). The quasiparticle number density is $\sim 5\%$ at $T \sim 35t$. Apparently, for higher temperatures the ideal gas picture is no longer valid as it crosses over to that of the strongly correlated normal liquid. We conclude that for large enough gaps and $T \lesssim 0.15\Delta$, one can rely on low temperature analytical predictions to do thermometry.

For smaller gaps, instead, we do not find any interesting region (i.e., where temperature effects are visible), for which the classical description is valid. In Fig. 8 we show the energy per particle as a function of temperature for $t/U = 0.025$ (the ground state is MI with the energy gap $\Delta = 18.35t$). To get the specific heat and entropy, we first use spline interpolation of the energy data points to obtain a smooth curve $E(T)$. The specific heat is then obtained by differentiating the spline. The maximum in the specific heat is reached when temperature is about half the energy gap. The entropy has been calculated by numerical integration of $c_V/T$. In order to see any temperature effect one has to go as high as $T \sim 2.5t$; at these temperatures the classical description is already no longer applicable and one has to rely on numerical data to do thermometry.

### B. Loading the optical lattice: Estimate of $T^{(\mathrm{fin})}$ from entropy matching

The standard approach to convert results obtained for a homogeneous system into predictions for systems in external

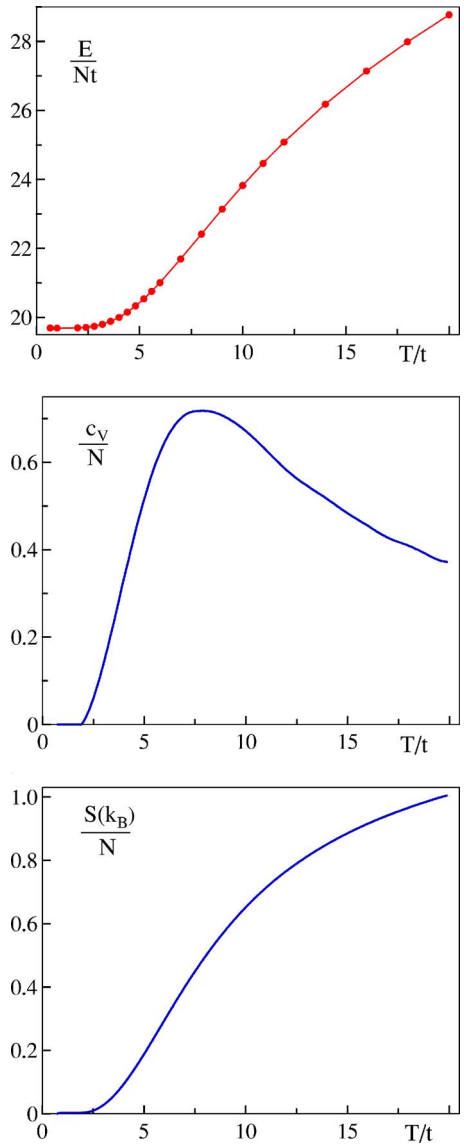


FIG. 8. (Color online) Energy (top), specific heat (middle), and entropy (bottom) per particle at $t/U=0.025$ (MI ground state) and unity filling factor. On the top, solid circles refer to prime data (error bars within symbol size). the data were taken for linear system sizes $L=10$ and 20. Within the error bars, we are not able to resolve any finite size effect. Solid lines in all plots are obtained from spline-interpolated data for energy, with subsequent analytic differentiation/integration of the interpolation curve.

fields is the so-called local density approximation (LDA), which is actually a local chemical potential approximation when the density at the site $i$ is identified with the density of the homogeneous system with the chemical potential

$$\mu_i^{(\mathrm{eff})} = \mu - V(i). \tag{11}$$

In strongly interacting regimes with a short healing and correlation length, the LDA approach can be easily justified in most cases (critical regions of phase transitions excluded). In Ref. 22, the authors directly compare simulation results for 1D and 2D harmonically trapped systems with LDA predictions based on known homogeneous system phase diagram.

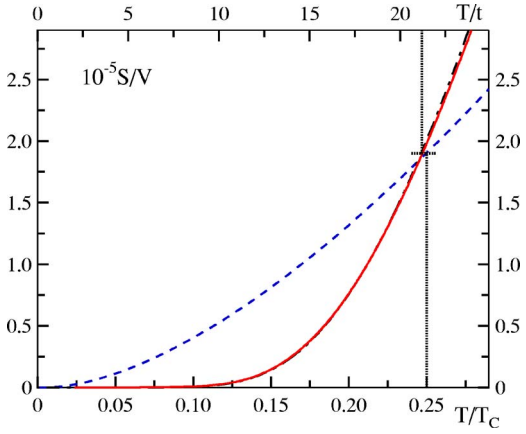


FIG. 9. (Color online) Entropy per particle at $t/U=0.005$, unity filling factor and linear system size $L=20$. The dashed line is the entropy of the uniform WIBG. The solid line is the result of analytical derivation/integration of numerical data for energy and the dashed-dotted line (barely visible) is the analytical prediction (12), where, at each temperature, the chemical potential has been fixed by the condition of having equal number of particle and hole excitations. If the system was initially cooled down to $T^{\text{in}}=0.25T_c$, the final temperature is $T^{\text{fin}}=22t$ and nearly a hundred of thermally activated particle-hole excitations are present in the final state (see inset in Fig. 7).

As expected, the density profiles differ only at the MI-SF interface, and we believe that the same will be true for the 3D case which is more "mean-field-like."

When the semianalytic predictions are reliable (see Fig. 7), one can use numerical results for the effective masses and gaps to calculate the entropy of the homogeneous quasiparticle gas with the tight-binding dispersion relation. The entropy is given by

$$S=-\frac{V}{(2\pi)^3}\int d^3\mathbf{k}\frac{\partial[\Omega_+(\mathbf{k})+\Omega_-(\mathbf{k})]}{\partial T}, \tag{12}$$

where

$$\Omega_\pm(\mathbf{k})=T\ln\left(1-\exp\frac{\epsilon_\pm(\mathbf{k})}{T}\right). \tag{13}$$

As an example, consider a uniform weakly interacting Bose gas (WIBG) of $^{87}$Rb with the gas parameter $na_s^3\sim10^{-6}$, which is loaded into an optical lattice with $\lambda=840$ nm and $t/U=0.005$. At low enough temperature, $T\lesssim0.3T_c$, one can calculate the initial (prior to imposing the lattice) entropy of the system using the Bogoliubov spectrum. In Fig. 9 we plot the entropy per unit volume before and after the optical lattice is imposed. The bottom $x$ axis is temperature in units of the critical temperature of the WIBG, the top $x$ axis is temperature in units of $t$, the hopping matrix element. The dashed line is the entropy of the WIBG, the solid and dashed-dotted lines represent the entropy of the Bose-Hubbard model calculated starting from the numerical results of Fig. 7 and analytical predictions of Eq. (12), respectively. If the system was prepared at $T\sim0.25T_c$, the final temperature would be $T\sim22t$. Figure 7 shows that at this temperature the system is quite far from its ground state and the number density of thermally activated particle-hole excitations is $\sim1\%$. The circumstances of this kind become crucial if one is to use the system in quantum information processing. This example is also illustrative of how numerical data can be used to suggest appropriate initial conditions.

Now we turn to a more realistic case of confined system and use LDA to convert results for the uniform system into predictions for the inhomogeneous one. In what follows, we consider a gas of $N\sim3\times10^4$ $^{87}$Rb atoms, magnetically trapped in isotropic harmonic potential of frequency $2\pi60$ Hz. Experiments with such number of particles were recently performed.[9] With this geometry, the parameter $\eta=1.57(N^{1/6}a_s/a_{ho})^{2/5}$ (see Ref. 23) is $\sim0.33$, which is a typical value in current experiments. For temperatures in the range $\mu<T<T_c$, where $T_c$ is the critical temperature of the harmonically trapped ideal gas, one can accurately calculate energy using the Hartree-Fock[24] mean field approach[25]

$$\frac{E}{NT_c}=\frac{3\zeta(4)}{\zeta(3)}t^4+\frac{1}{7}\eta(1-t)^{2/5}(5+16t^3), \tag{14}$$

where $t$ is the reduced temperature $T/T_c$. At very low T ($T<\mu$), Eq. (14) misses the contribution coming from collective excitations. We are interested in initial temperatures $T\sim0.2-0.3T_c$, which are feasible in current experiments.[26] Starting from Eq. (14), we calculate the entropy of the BEC initially prepared in the magnetic trap. After the optical lattice is adiabatically turned on, the magnetic potential provides a scan over the chemical potential of the homogeneous system [see Eq. (11)].

A direct comparison with experiments at fixed number of particles would require to calculate $\mu(T)$ from the normalization condition. At low temperatures, one expects the dependence of the chemical potential on temperature to be weak (this will be confirmed by direct simulations, see below). For simplicity, we fix $\mu$ at a value corresponding to $N=30^3$ trapped atoms in the first Mott lobe, at zero temperature. From this point we proceed in two directions. On one hand, we analytically calculate the low temperature contribution to energy and entropy arising from particle and hole excitations in the trapped MI state. On the other hand, we directly simulate the thermodynamics of the inhomogeneous system at a fixed chemical potential. The results are shown in Fig. 10, where we plot the energy per particle, counted from the ground state. The solid circles are data from the simulations (error bars are plotted), the solid line is the (analytically calculated) contribution of the particle and hole excitations. The inset shows the low temperature region. A large mismatch between the two results indicates that the main contribution to energy is given by the liquid at the perimeter of the trap. At zero temperature, there are about $N\sim29\,000$ particles in the trap, 7% of which are not in the MI state (recall that $\mu$ has been determined by placing $30^3$ particles in the MI state). Simulation results show that, in the range of temperatures considered, the total number of particles increases by 0.7% at most, which confirms the weak temperature dependence of the chemical potential. In addition, for $T=8t$, we performed a simulation with $N$ fixed at the ground state value. The energies per particle in the canonical and grand canonical simu-

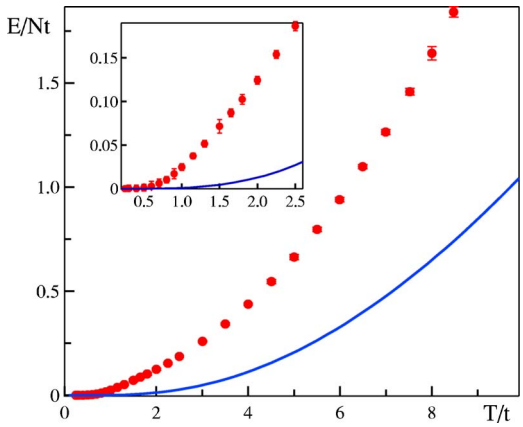


FIG. 10. (Color online) Energy per particle at $t/U=0.005$, $\mu=116.5t$, and trap frequency $\omega=2\pi 60$ Hz. Solid circles are numerical data, the solid line is the energy of particle and hole excitations in MI deduced from Eq. (7). The inset shows a zoom of the low temperature range. At $T\sim 2.3t$ the contribution of MI excitations to energy is $\sim 10\%$ only.

lations differ by 0.3% only, therefore we proceed calculating the entropy in the canonical ensemble and compare it with the initial entropy of the system, at a fixed particle number.

We are in a position to address the question of what is the final temperature of the system after the optical lattice is turned on and the final state is MI with the exception of a small shell at the trap perimeter. In Fig. 11 we plot the entropy of the trapped WIBG with (solid line) and without (dashed line) the optical potential. If the initial system is cooled down to temperatures $T^{(\mathrm{in})}\sim 0.25T_c$, see, e.g., Ref. 26, the final temperature will be $T^{(\mathrm{fin})}=(2.35\pm 0.30)t$.

With the initial conditions considered in this example, what is the final state of the liquid at the perimeter of the trap? Before answering this question, we would like to recall that, along the MI-SF transition lines, the critical temperature for the normal-to-superfluid transition is zero. The transition

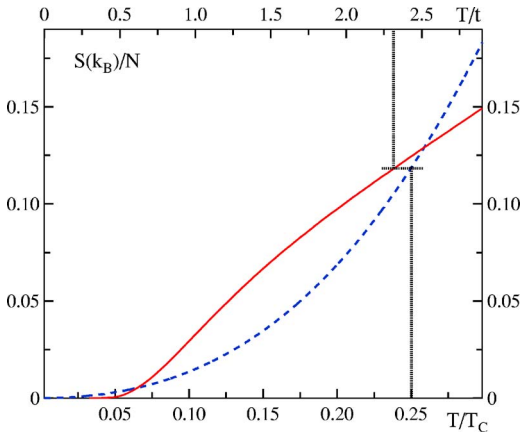


FIG. 11. (Color online) Entropy per particle for the same system as in Fig. 10. The dashed line is the entropy of the trapped WIBG, before the optical lattice is loaded; the solid line is the final entropy. If the system was initially cooled down to $T^{(\mathrm{in})}=0.25T_c$, the final temperature is $T^{(\mathrm{fin})}=(2.35\pm 0.3)t$ and the liquid at the perimeter of the trap is normal (see text).

temperature increases as one moves away from the border of the Mott lobes (lowering $\mu$ at fixed $t/U$ in our case) and the quasiparticle density increases until it reaches its maximum at about $n\approx 1/2$ and then decreases. The maximum $T_c$ can be estimated from the ideal Bose gas relation $T_c^{(0)}=3.313n^{2/3}/m^*=4.174t$, with $n=0.5$ and $m^*=1/2t$, but interaction effects are likely to reduce this value. We have performed simulations at half filling factor and fixed $t/U=0.005$, and found the critical temperature to be $T_c(n=1/2)=2.09(1)t$. As a consequence, for the chosen initial conditions, we can conclude that the final state of the liquid at the perimeter of the trap is normal and it gives the main contribution to the entropy. For such low final temperature, the contribution to the entropy per particle due to thermally activated excitations in the MI state is only 10%. The largest chemical potential is, in fact, deep in the first Mott lobe, and the energy required to introduce an extra particle or hole is much larger than $T$. Most excitations are located at the perimeter of the Mott state in a narrow shell of radius $R$ and width $\sim 0.05R$.

Retrieving the same information for experiments using a larger number of particles, e.g., $10^5-10^6$, by direct simulation is still computationally challenging. In order to use LDA, one should study the uniform system, scanning through the chemical potential. As our last example, we consider a uniform system which is in the correlated SF ground state. Figure 12 shows data for $E$, $c_V$, and $S$ for $t/U=0.0385$ and unity filling factor, close to the MI-SF transition. The system stays in its ground state for $T\ll 2t$; in finite systems, the energy of the lowest mode is finite $E_{\min}=cp_{\min}$ (with $c\approx 6t$ and $p_{\min}=2\pi/L$). The specific heat and entropy are calculated as described for Fig. 8. We were not able to resolve the SF-NL transition temperature from this set of data alone: numerical data corresponding to system sizes $L=10$ and $L=20$ overlap within error bars and we did not see any feature at the critical temperature. This is not surprising since the specific heat critical exponent $\alpha$ is very small, and it is thus very difficult to resolve the singular contribution and finite size effects in energy and specific heat. For a system of linear size $L$, the singular part of the specific heat $c_V^{(s)}$ can be written as

$$c_V^{(s)}(t,L)=\xi^{\alpha/\nu}f_c(\xi/L)=L^{\alpha/\nu}g_c(tL^{1/\nu}), \tag{15}$$

where $t=(T-T_c)/T_c$, $\alpha\approx -0.01$, $\nu=(2-\alpha)/3$, $\xi$ is the correlation length, and $f_c(x)$ and $g_c(x)$ are the universal scaling functions. At the critical point, finite size effects for the two system sizes considered are $\sim 1\%$, within error bars.

The critical temperature was extracted from data for the superfluid stiffness. The scaling of the superfluid stiffness at the critical temperature is $n_s\propto |t|^{\nu}$. This allows one to accurately estimate the critical temperature from

$$n_s(t,L)=\xi^{-1}f_s(\xi/L)=L^{-1}g_s(tL^{1/\nu}), \tag{16}$$

by plotting $n_sL$ vs $T$ as shown in Fig. 13. From the data taken for system sizes $L=5$, $L=10$, $L=20$, we estimate the critical temperature to be $T_c=3.25(1)t$. At this temperature, the entropy per unit particle is $\sim 0.195$, or, translating to entropy density in physical units, $3.6\times 10^{-5}$ J K$^{-1}$ m$^{-3}$, which corre-

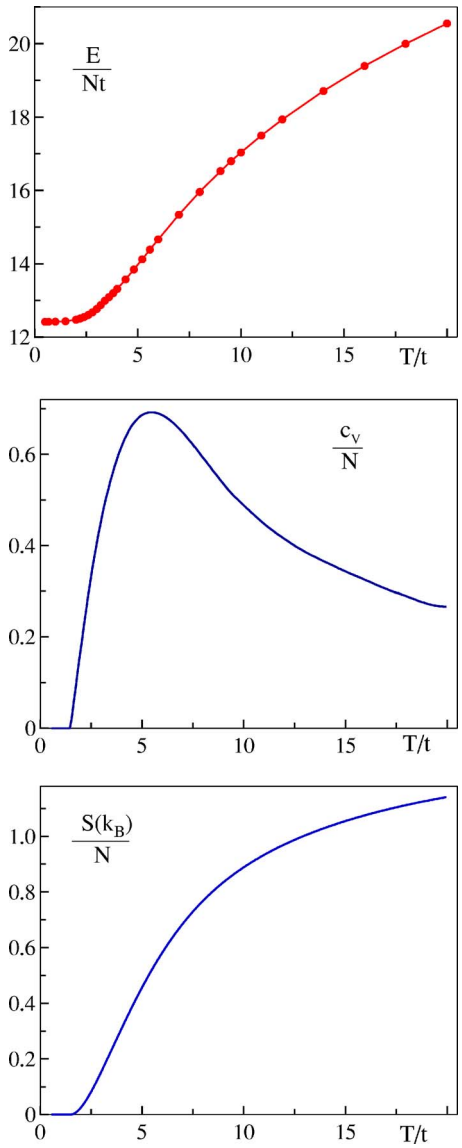


FIG. 12. (Color online) Energy (top), specific heat (middle), and entropy (bottom) per particle at $t/U=0.0385$ (SF ground state) and unity filling factor. On the top, solid circles refer to prime data (error bars within symbol size). Data were taken for system size $L=10$ and 20. Within error bars, we are not able to resolve any finite size effect. Solid lines in all plots are obtained from spline-interpolated data for energy, with subsequent analytic differentiation/integration of the interpolation curve.

sponds to an initial temperature $\sim 0.35 T_c^{(\mathrm{in})}$. Therefore it seems plausible to reach $T_c$ experimentally.

The results shown in Fig. 1 were determined using the procedure described above. A similar figure already exists in literature, see Ref. 19, where the authors carry on a slave fermions/bosons mean field approach to calculate the critical temperature as a function of $U/t$. Results from the four body slave fermion approach are comparable to our numerical results in the range $U/t \lesssim 24$, that is, in the weakly interacting and intermediate regime. In the vicinity of the critical point, though, the mean field results are not accurate and the prediction for the zero temperature $(U/t)_c$ is $\sim 20\%$ higher than the numerical one.

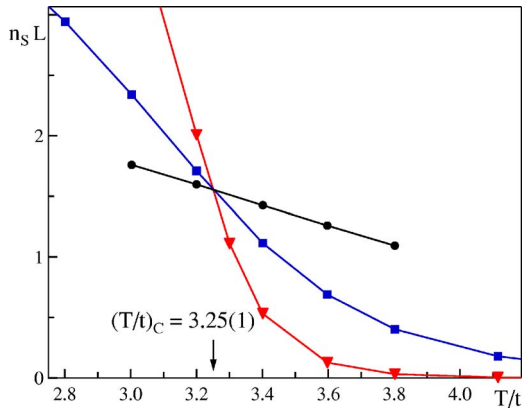


FIG. 13. (Color online) Finite size scaling of the superfluid stiffness. $n_s L$ vs $T/t$ for system size $L=5$ (circles), $L=10$ (squares), $L=20$ (triangles). We estimate the critical temperature to be $T_c=3.25(1)t$, already nearly half the noninteracting gas value.

## IV. CONCLUSIONS

We have performed quantum Monte Carlo simulations of the three dimensional homogeneous Bose-Hubbard model. We were able to establish the phase diagram of the MI-SF transition with the record accuracy $\sim 0.1\%$ and determine the size of the fluctuation region in the vicinity of the diagram tip where universal properties of the relativistic effective theory can be seen. Comparison with the strong-coupling expansion shows that the latter works well only for sufficiently large insulating gaps $\Delta > 6t$ outside of the fluctuation region. We have studied the effective masses of particle and hole excitations along the MI-SF boundary. Our results directly demonstrate the emergence of the particle-hole symmetry at the diagram tip, and provide base for accurate theoretical estimates of the MI thermodynamics at low and intermediate temperatures.

We have studied thermodynamic properties of the superfluid and insulating phases at fixed particles number for the uniform case. These data can be used to make predictions for the inhomogeneous system using the local density approximation. We have shown that for large enough gaps the low temperature analytical predictions agree with numerical data. By entropy matching, we have calculated the final temperature of the system (after the optical lattice is adiabatically loaded), in the uniform and magnetically trapped system, at $t/U=0.005$. We have performed direct simulations of a trapped system, using typical experimental values for the magnetic potential and number of particles. For the initial conditions considered, we found the final temperature and demonstrated that the main contribution to the entropy comes from the liquid at the perimeter of the trap. We have calculated the normal-to-superfluid transition temperature at half filing and concluded that the liquid at the perimeter is normal.

## ACKNOWLEDGMENTS

We are grateful to Matthias Troyer for useful discussions. This work was supported by the National Science Foundation Grant No. PHY-0426881.

[1] D. Jaksch and P. Zoller, Ann. Phys. (N.Y.) **315**, 52 (2005).
[2] M. P. A. Fisher, P. B. Weichman, G. Grinstein, and D. S. Fisher, Phys. Rev. B **40**, 546 (1989).
[3] D. Jaksch, C. Bruder, J. I. Cirac, C. W. Gardiner, and P. Zoller, Phys. Rev. Lett. **81**, 3108 (1998).
[4] M. Greiner, O. Mandel, T. Esslinger, T. W. Haensch, and I. Bloch, Nature (London) **415**, 39 (2002).
[5] G. G. Batrouni, V. Rousseau, R. T. Scalettar, M. Rigol, A. Muramatsu, P. J. H. Denteneer, and M. Troyer, Phys. Rev. Lett. **89**, 117203 (2002).
[6] F. Gerbier, A. Widera, S. Folling, O. Mandel, T. Gericke, and I. Bloch, Phys. Rev. A **72**, 053606 (2005).
[7] A. Isacsson, Min-Chul Cha, K. Sengupta, and S. M. Girvin, Phys. Rev. B **72**, 184507 (2005).
[8] S. Fölling, A. Widera, T. Müller, F. Gerbier, and I. Bloch, Phys. Rev. Lett. **97**, 060403 (2006).
[9] F. Gerbier, S. Fölling, A. Widera, O. Mandel, and I. Bloch, Phys. Rev. Lett. **96**, 090401 (2006).
[10] S. R. Clark and D. Jaksch, New J. Phys. **8**, 160 (2006).
[11] *Atom Interferometry*, edited by P. Berman (Academic Press, New York, 1997).
[12] J. A. Dunningham and K. Burnett, Phys. Rev. A **70**, 033601 (2004).
[13] J. A. Dunningham, K. Burnett, and S. M. Barnett, Phys. Rev. Lett. **89**, 150401 (2002).
[14] M. Rodríguez, S. R. Clark, and D. Jaksch, Phys. Rev. A **75**, 011601(R) (2007).
[15] J. K. Freericks and H. Monien, Phys. Rev. B **53**, 2691 (1996).
[16] N. V. Prokof'ev, B. V. Svistunov, and I. S. Tupitsyn, Phys. Lett. A **238**, 253 (1998); JETP **87**, 310 (1998).
[17] M. R. Andrews, C. G. Townsend, H. J. Miesner, D. S. Durfee, D. M. Kurn, and W. Ketterle, Science **275**, 637 (1997).
[18] W. Ketterle, D. S. Durfee, and D. M. Stamper-Kurn, in *Proceedings of the International School of Physics–Enrico Fermi*, edited by M. Inguscio, S. Stringari, and C. E. Wieman (IOS Press, Amsterdam, 1999), p. 67.
[19] Y. Yu and S. T. Chui, Phys. Rev. A **71**, 033608 (2005).
[20] V. A. Kashurnikov, N. V. Prokof'ev, and B. V. Svistunov, Phys. Rev. Lett. **87**, 120402 (2001).
[21] V. A. Kashurnikov, N. V. Prokof'ev, B. V. Svistunov, and M. Troyer, Phys. Rev. B **59**, 1162 (1999).
[22] S. Wessel, F. Alet, M. Troyer, and G. G. Batrouni, Phys. Rev. A **70**, 053615 (2004).
[23] S. Giorgini, L. P. Pitaevskii, and S. Stringari, Phys. Rev. Lett. **78**, 3987 (1997).
[24] V. V. Goldman, I. F. Silvera, and A. J. Leggett, Phys. Rev. B **24**, 2870 (1981); D. A. Huse and E. D. Siggia, J. Low Temp. Phys. **46**, 137 (1982).
[25] F. Dalfovo, S. Giorgini, L. P. Pitaevskii, and S. Stringari, Rev. Mod. Phys. **71**, 463 (1999).
[26] F. Gerbier, J. H. Thywissen, S. Richard, M. Hugbart, P. Bouyer, and A. Aspect, Phys. Rev. A **70**, 013607 (2004).